Optik 144 (2017) 9–14

Contents lists available at ScienceDirect

Optik

journal homepage: www.elsevier.de/ijleo

Original research article

Real-time wavefront reconstruction for extended object based on phase diversity

Dan Yue[a,*], Ye Li[a], Haitao Nie[b], Guangyong Jin[a]

[a] Changchun University of Science and Technology, Changchun 130022, China
[b] Changchun Institute of Optics, Fine Mechanics and Physics, Chinese Academy of Sciences, Changchun 130033, China

ARTICLE INFO

Article history:
Received 23 March 2017
Accepted 19 June 2017

OCIS Codes:
010.735
100.5070
110.1080
120.4820

Keywords:
Wave-front sensing
Wave-front sensing
Active or adaptive optics
Phase diversity
Image reconstruction-restoration

ABSTRACT

We present a real-time solution to the phase diversity problem when the observed objects are extended scenes. It utilizes an iterative linearization of the optical transfer functions (OTF) in at least two diversity planes by a first-order Taylor expansion to reconstruct initial wavefront. Vast simulation experiments are processed to verify the presented algorithm, including comparing our algorithm with the analytic estimator method, demonstrating that our method has high wavefront detection accuracy and large linearity range.

Introduction

Since the inception of phase diversity (PD) about two decades ago, many authors have used the PD method [1–5], which utilizes at least two images of the same object recorded in presence of a known optical aberration (e.g. defocus), to estimate the wavefront of optical systems and enhance the detected image. The hardware of PD technique is limited to or can be merged in the usual imaging sensor, the number of estimated modes can be continuously tuned and it is among the very few methods enabling the measurement of differential pistons, tip-tilts on segmented or divided apertures. However, the main drawback of classic PD is that since it is a nonlinear optimization problem, complexity is reported on data processing. Due to the high computational complexity and possible convergence to local optima [6], the nonlinear PD has a limited usage in real-time correction algorithms.

Considerable effort has been directed toward decreasing the computational complexity of the PD algorithm. The common idea is to linearize the generalized pupil function (GPF) or point spread function (PSF) based on the assumption that the total aberration is small, such as paper [7–9] utilize an expansion of the GPF to retrieve the unknown phase and paper [10,11] linearize PSF to reconstruct the wavefront. But all of them need a single point source, and thus cannot be operated on observation systems which take images of very extended scenes. Paper [12] presented an approximation of optical transfer function (OTF) which can be used for the detection of wavefront aberrations on extended object, but is limited to extremely

* Corresponding author.
E-mail address: danzik3@126.com (D. Yue).

http://dx.doi.org/10.1016/j.ijleo.2017.06.064
0030-4026/

small phase aberrations. In this letter, we present a real-time wavefront reconstruction for extended object by the use of the iterative linearization of OTFs in at least two diversity planes and compare with the analytic estimator method proposed in paper [12]. The experimental results demonstrate that our method effectively increases the linearity range, making it much larger than that in paper [12].

We first present the model for image formation through the optical system in the presence of aberrations. The phase aberrations $\phi_k \in \mathbb{R}^{m^2\times 1}$ in the k-th diversity image can be approximated using a normalized Zernike basis [13]:

$$\phi_k(u_j, v_j) = Z(u_j, v_j)(\alpha + \beta_k), \tag{1}$$

where m^2 is the number of pixels, $\alpha \in \mathbb{R}^{n\times 1}$ is the n Zernike coefficients to be reconstructed, $\beta_k \in \mathbb{R}^{n\times 1}$ is the introduced known diversity to eliminate the ambiguity of the inverse problem, $Z(u_j, v_j) \in \mathbb{R}^{m^2\times n}$ is the matrix of the n Zernike polynomials evaluated in the pupil plane (u_j, v_j) coordinates. These phase aberrations nonlinearly influence the PSF expressed in the spatial coordinates (s_j, t_j), which can be written as:

$$h(s_j, t_j; \alpha, \beta_k) = |\Im\left[P(u_j, v_j)\exp(i\phi_k(u_j, v_j))\right]|^2(s_j, t_j), \tag{2}$$

where $\Im$ is the Fourier transform and P is the binary pupil function.

The image recorded at the k-th optical plane of an instrument is modeled by the discrete and noisy convolution of the PSF with the observed object, shown as:

$$y_{k,j}(s_j, t_j) = o * h(s_j, t_j; \alpha, \beta_k) + n_k(s_j, t_j), \tag{3}$$

where $y_{k,j}$ denotes the j-th pixel of the k-th diversity image, o is the true observed object and $n_k(s_j, t_j)$is additive noise. Eq. (3) can be rewritten in frequency domain as below:

$$Y_{k,j}(f_{s_j}, f_{t_j}) = \mathrm{O} \bullet \mathrm{S}(f_{s_j}, f_{t_j}; \alpha, \beta_k) + N_k(f_{s_j}, f_{t_j}), \tag{4}$$

where $Y_{k,j}$, O, S and N_k are discrete Fourier transforms of $y_{k,j}$, o, h and n_k, respectively, $(f_s\ \ j, f_t\ \ j)$ is the coordinate vector in the frequency domain and $\bullet$ denotes the dot product. We introduce the short-hand notations of $S(f_s\ \ j, f_t\ \ j; \alpha, \beta_k)$as $S_j(\alpha, \beta_k)$, recall that $S_j(\alpha, \beta_k)$ is the OTF of the k-th image plane.

We approximate the OTF by a first order Taylor expansion for small aberrations and non-zero diversities. The first-order Taylor approximation of the OTF in $\alpha = 0$ is given by:

$$S_j(\alpha, \beta_k) = D_{0,j}(\beta_k) + D_{1,j}(\beta_k)\alpha + O\|\alpha\|^2, \tag{5}$$

where$D_{0,j}(\beta_k) = S_j(\alpha, \beta_k)|_{\alpha=0}$, $D_{1,j}(\beta_k) = \frac{\partial S_j(\alpha,\beta_k)}{\partial\alpha}|_{\alpha=0}$ and $O\|\alpha\|^2$is the 2-th order Lagrange residue.

In order to eliminate the unknown object to establish a direct relationship between the detected images and the unknown aberrations, two images Y_1 and Y_2 are used here based on PD technique. Multiplying them by each other's OTF, thus we get Eqs. (6) and (7):

$$S_2 \bullet Y_1 = S_2 \bullet O \bullet S_1 + S_2 \bullet N_1, \tag{6}$$

$$S_1 \bullet Y_2 = S_1 \bullet O \bullet S_2 + S_1 \bullet N_2. \tag{7}$$

Since these two equations only involving dot product, we can eliminate the unknown object by subtracting these two image measurements, shown as below:

$$S_2 \bullet Y_1 - S_1 \bullet Y_2 = S_2 \bullet N_1 - S_1 \bullet N_2. \tag{8}$$

Substituting Eq. (5) into this expression and abandoning 2-th order residue yields a new estimate of phase via the solution of a least-square (LS) problem:

$$Y = A\alpha + \Delta N, \tag{9}$$

where

$Y = D_{0,j}(\beta_1) \bullet Y_2 - D_{0,j}(\beta_2) \bullet Y_1$, $\mathrm{A} = D_{1,j}(\beta_2) \bullet Y_1 - D_{1,j}(\beta_1) \bullet Y_2$, $\Delta\mathrm{N} = S_1 \bullet N_2 - S_2 \bullet N_1$

Thus, the linear estimate of the phase aberrations can be obtained by the LS estimator:

$$\alpha = \left[\Re(A^T A)\right]^{\dagger}\left[\Re(A^T Y)\right], \tag{10}$$

where $\bullet^T$ denotes the transposition, $\Re$ represents the real part operator and $\bullet^{\dagger}$ is the generalized inverse of a matrix.

We consider only the static setting, where the aberrations do not change in the time window considered. We start with an initial estimate of α using the OTF approximation around zero aberration, then a new linearization of the OTF can be done around the current phase estimate $\hat{\alpha}$ and a new least squares (LS) problem can be established to solve the next estimate. We repeat the process until reach the number of iteration times or the norm of the aberration increment reach the set threshold,

Table 1
Aberrations Applied over the Configuration.

Actual coefficients of co-phase errors (λ)			
	Piston	Tip	Tilt
Sub-aperture 1	0	0	0
Sub-aperture 2	−0.0025	−0.2239	0.2939
Sub-aperture 3	−0.2896	0.0022	0.0652
Sub-aperture 4	−0.1363	0.1930	0.1587
Sub-aperture 5	−0.1568	0.1075	0.0716
Sub-aperture 6	0.0848	−0.2988	−0.1734

namely $\|\hat{\alpha}_{i+1} - \hat{\alpha}_i\| \le \varepsilon$ (e.g. $\varepsilon = 10^{-6}$). Once we obtain the phase aberrations, the observed object can be recovered by the classic PD algorithm:

$$O = \frac{\sum_{k=1}^{K} Y_k S_k^*}{\sum_{k=1}^{K} |S_k|^2 + \gamma}, \tag{11}$$

with $\bullet^*$ conjugation and γ the nonnegative regularization parameter.

In order to verify our algorithm, we apply it to co-phase the segmented optical system, which is removing misalignments resulting from relative piston aberrations between segments and tip-tilt aberrations of each segment. We assume the instrument pupil is composed by T identical apertures, each sub-aperture has a complex transmission p_t and corresponding phase ϕ_t, thus the aperture function of the telescope can be written as:

$$P(\mathbf{u}) = \sum_{t=1}^{T} p_t(\mathbf{u} - \mathbf{u_t}) \exp[i\phi_t(\mathbf{u} - \mathbf{u_t})], \tag{12}$$

where $\mathbf{u}$ is the position vector in the aperture plane and $\mathbf{u_t}$ is the segment center point. As we only deal with piston and tip-tilt, thus the phase can be expanded on the first three terms of scaled Zernike polynomials:

$$\phi_t(\mathbf{u} - \mathbf{u_t}) = 2\pi \left(\sum_{t=1}^{T} \sum_{s=1}^{3} \alpha_{ts} Z_s(\mathbf{u} - \mathbf{u_t}) \right), \tag{13}$$

where α_{ts} is the s-th coefficient of the t-th sub-aperture phase aberration in terms of wavelength.

Utilizing the relationships between the OTF, PSF and the GPF in incoherent imaging systems, we can obtain the PSFs and OTFs in each diversity plane of the segmented optical system based on Eq. (12). Here we directly give the first order partial differential of the k-th OTF with respect to the coefficient α_{ts}:

$$\frac{\partial S_k}{\partial \alpha_{ts}} = \Im\{2\Re\left[\Im\{i2\pi Z_s p_t \exp(i\phi_t)\exp(i\phi_{dk})\} \cdot h_k^*\right]\}. \tag{14}$$

Thus, the derivative of OTFs can be computed based on current phase estimate at each iteration. We can also use the difference to calculate the derivative of the OTFs.

Using 6 hexagon sub-aperture and set one of the sub-apertures as standard, we apply a set of random piston and tip-tilt restricted in $\pm 0.3\lambda$ listed in Table 1 to all sub-apertures. We consider the pupil of radius r sampled on a 64×64 grid embedded in a $4r \times 4r$ image to satisfy the Nyquist sampling criterion. The observed object is an urban scene, monochromatic images of size $N_{pix} = 256 \times 256$ pixels are simulated with intensity-dependent Poisson-distributed photon noise plus zero-mean, additive Gaussian CCD readout noise with a standard deviation of 15 e^-. The average pixel signal-to-noise ratio (SNR) is defined as:

$$SNR = \frac{1}{m^2} \sum_{j=1}^{m^2} \frac{g(s_j, t_j)}{\sqrt{g(s_j, t_j) + \sigma_{read}^2}}, \tag{15}$$

where m^2 is the number of pixels, $g(s_j, t_j)$ is the noise free image and σ_{read}^2 is the variance associated with the read noise.

Two images are recorded here in two observation planes, one at focal plane and the other with a 1λ peak-to-valley (PV) defocus amount. Fig. 1 shows the corresponding simulated images with peak pixel intensity 3000 e^-, namely SNR = 32.06.

We show the convergence of the algorithms for the particular wavefront in Table 1 in the noiseless case and the specific noise level (with SNR = 32.06) based on the two corresponding images. The results are shown in Table 2, which list the residual RMS values on the phase estimates obtained after each iteration for the two noise cases. Here, we define the residual RMS value on the phase estimates as $\left[\sum_{t=1}^{T}\sum_{s=1}^{3}\langle\left(\hat{\alpha}_{ts} - \alpha_{ts}^{true}\right)^2\rangle\right]^{1/2}$.

Table 2 shows that the appearance of noise leads to more iteration times and larger residual errors of phase estimates.

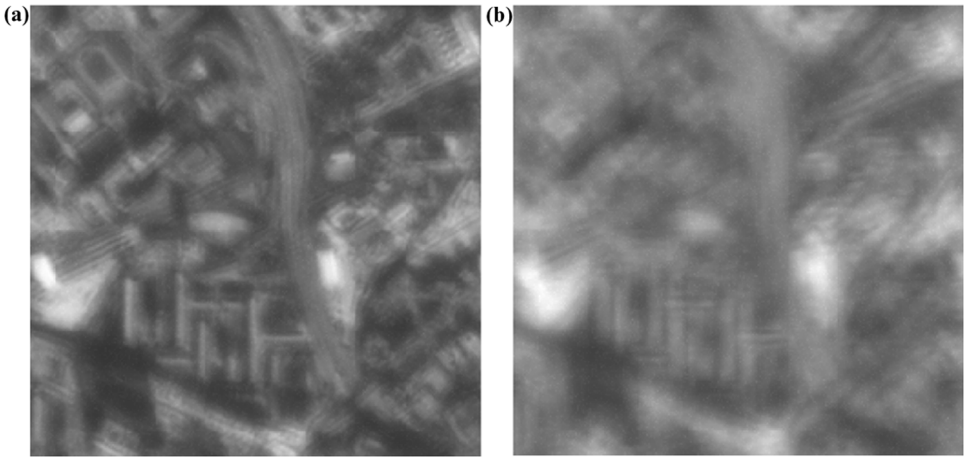

Fig. 1. Corresponding (a) in-focus and (b) out-of-focus images under SNR = 32.06.

Table 2
Residual RMS Values (λ) Obtained After Each Iteration for the Two Noise Levels, and 0.1777λInitial RMS.

Noise (SNR)	Iterations				
	0	1	2	3	4
∞	0.1777	0.1433	0.0733	0.0499	2.2742 e-04
32.06	0.1777	0.1451	0.0756	0.0615	0.0242

Noise (SNR)	Iterations			
	5	6	7	8
∞	5.3789 e-08	–	–	–
32.06	0.0089	0.0034	0.0010	9.0257 e-04

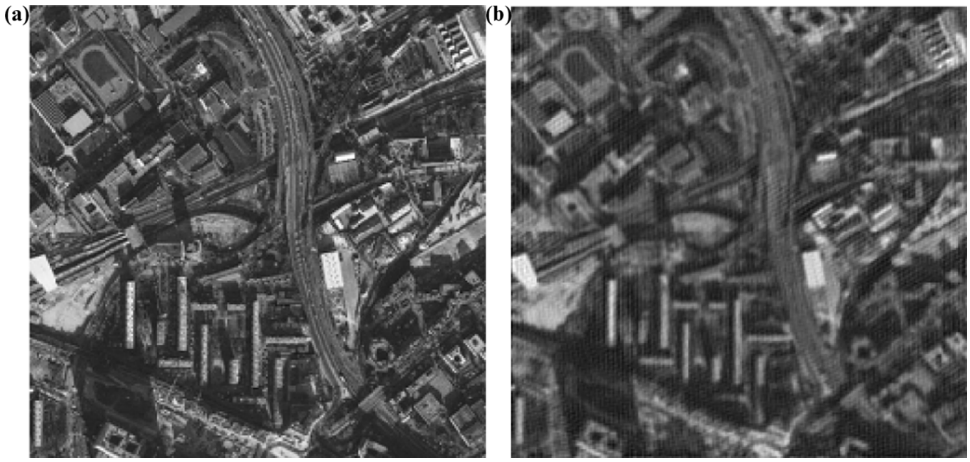

Fig. 2. Recovered observed object (a) noise free situation and (b) with SNR = 32.06.

The recovered urban scene under the two noise cases are shown in Fig. 2. We define the RMS values on the object estimate as $\left[\sum_1^{m^2}\langle\left(\hat{o}-o_{true}\right)^2\rangle\right]^{1/2}/\left[\sum_1^{m^2}o_{true}^2\right]^{1/2}$, where $\hat{o}$ and o_{true} are the recovered object and true observed object, respectively. The RMS values of Fig. 2 (a) and (b) are 9.23% and 16.71%, respectively.

We now repeat the experiment in the previous section for random wavefront aberrations restricted in $\pm 0.5\lambda$, corresponding distorted phase limited to 2π rad, using our method (marked as M2) and compare with the analytic estimator method in paper [12] (marked as M1). For each range of PV values of the initial aberration coefficients, the experiments are repeated 100 times for both M1 and M2. We use errorbars to visualize the results. Fig. 3 shows the contrast experimental results

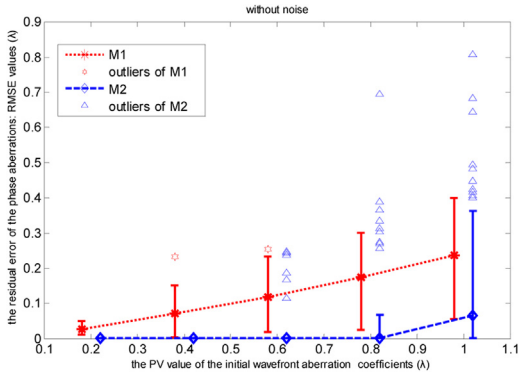

Fig. 3. Contrast plots of the residual error of the phase estimates with respect to increasing PV value of the initial wavefront aberrations without noise.

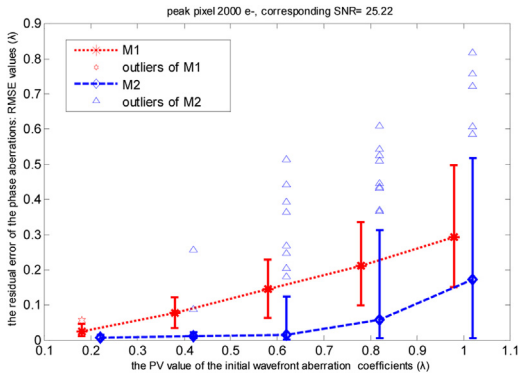

Fig. 4. Contrast plots of the residual error of the phase estimates with respect to increasing PV value of the initial wavefront aberrations with SNR = 25.22.

Table 3
Number of Photons in Peak Pixel and Corresponding SNRs.

	Noise added: photon noise, readout noise				
Peak pixel photons (e^-)	500	1000	1500	3000	5000
Average pixel SNR	9.84	16.18	21.09	32.06	42.75

totally without noise, in which we plot the residual error RMS values of the phase estimates with respect to the increasing PV value of initial wavefront aberrations. On each bar, the in-between mark is the mean value, the edges of the bars are the minima and maximum after getting rid of the outliers. The data equal or greater than 2 times of the original mean value are defined as outliers, which are plotted individually in the form of scatter. The same type of analysis is made in Fig. 4, which shows the contrast experimental results when the intensity of simulated image is 2000 e^- peak pixel, corresponds to SNR = 25.22.

Form Figs. 3 and 4, we can see that our method has much wider wavefront detection range but has more outliers than M1. This is because we utilize an iterative linearization expansion which can broaden the detection range, but also iteratively increases residual error if the estimate direction is not right. But in general, our method has far better performance on the linearity range than the analytic estimator method in paper [12] with or without noise.

We also compare our method with paper [12] under different noise level for a specific initial wavefront aberration within $\pm 0.2\lambda$. Table 3 shows the peak pixel photon count and corresponding average pixel SNRs. For each SNR, we repeat the experiment 100 times for both methods. The considered initial aberration has 0.13λ RMS. Fig. 5 plots the contrast residual errors on the phase estimates after correction versus increasing SNRs for both M1 and M2 in the form of errorbars. The outliers are also plotted individually.

Fig. 5 shows that our method has much higher wavefront detection accuracy than M1 when the noise level is not extremely high.

As a conclusion, we have presented an iterative linearization algorithm to realize real-time wavefront reconstruction for extended observed object. It utilizes a first-order Taylor expansion to linearize the OTFs of both diversity planes and establish a linear relationship between the detected images and the unknown wavefront aberrations. The experimental results shows that this algorithm can typically estimate the wavefront aberrations up to 0.6λ PV value with an error of $\lambda/70$ even under high noise level. The iteration times are 6 and 10 for noise free and noisy cases under good conditions, which consume

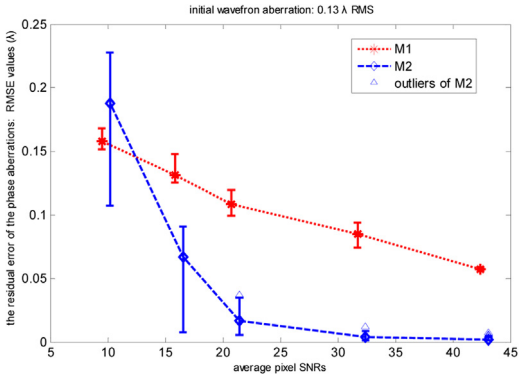

Fig. 5. Contrast plots of the residual error of the phase estimates with respect to increasing SNR with 0.13λ RMS initial wavefront aberration.

2.456 s and 3.806s, respectively. The computer employed for these simulations is a 3.2 GHz Intel (R) Core (TM) i5-4570 CPU with 4.0 GB of RAM. Thus we can conclude that the presented method can be used for real-time wavefront correction when the observed object is extended scene.

Acknowledgement

This work was supported by National Natural Science Foundation of China (No. 61205143).

References

[1] R.G. Paxman, J.R. Fienup, Optical misalignment sensing and image reconstruction using phase diversity, J. Opt. Soc. Am. A 5 (1988) 914–923.
[2] R.G. Paxman, T.J. Schultz, J.R. Fienup, Joint estimation of object and aberrations by using phase diversity, J. Opt. Soc. Am. A 9 (1992) 1072–1085.
[3] Q. Li, S. Liao, H.G. Wei, et al., Restoration of solar and star images with phase diversity-based blind deconvolution, Chin. Optic. Lett. 5 (4) (2007) 201–203.
[4] H. Mao, X. wang, D.Z. Zhao, Application of phase-diverse phase retrieval to wavefront sensing in non-connected complicated pupil optics, Chin. Optic. Lett. 5 (7) (2007) 397–399.
[5] Q. Cheng, Precise alignment of off-axis three-mirror reflecting optical system based on phase diversity, Chin. Optic. Lett. 13 (2015) (Suppl.): S11003-1- S11003-4.
[6] D.R. Gerwe, M.M. Johnson, B. Calef, Local minima analysis of phase diverse phaseretrieval using maximum likelihood, in: AMOS Technical Conference, Kihei HI, 2008.
[7] W.J. Wild, Linear phase retrieval for wave-front sensing, Opt. Lett. 23 (8) (1998) 573–575.
[8] R.A. Gonsalves, Small-phase solution to the phase-retrieval problem, Opt. Lett. 26 (10) (2001) 684–685.
[9] C.U. Keller, V. Korkiakoski, N. Doelman, R. Fraanje, R. Andrei, M. Verhaegen, Extremely fast focal-plane wavefront sensing for extreme adaptive optics, Proc. SPIE 8447 (2012) 21.
[10] S. Meimon, T. Fusco, L.M. Mugnier, LIFT: a focal-plane wavefront sensor for real-time low-order sensing on faint sources, Opt. Lett. 35 (18) (2010) 3036–3038.
[11] C.S. Smith, R. Marinică, A.J. Den Dekker, M. Verhaegen, V. Korkiakoski, C.U. Keller, N. Doelman, Iterative linear focal-plane wavefront correction, J. Opt. Soc. Am. A 30 (10) (2013) 2002–2011.
[12] I. Mocoeur, L.M. Mugnier, F. Cassaing, Analytical solution to the phase-diversity problem for real-time wavefront sensing, Opt. Lett. 34 (22) (2009) 3487–3489.
[13] ANSI, Methods for Reporting Optical Aberrations of Eyes, American National Standard for Ophtalmics ANSI-Z80, 2004, 28–2004.